Sensors and Actuators B 263 (2018) 281–288

Contents lists available at ScienceDirect

Sensors and Actuators B: Chemical

journal homepage: www.elsevier.com/locate/snb

Precision guided microfluidic chemical perfusion strategy for cell dynamic imaging

Peng Chen [1], Xiaojun Feng [1], Shuangqian Yan, Yiran Guo, Jie Wang, Yiwei Li, Dongjuan Chen, Wei Du, Bi-Feng Liu *

The Key Laboratory for Biomedical Photonics of MOE, Wuhan National Laboratory for Optoelectronics-Hubei Bioinformatics & Molecular Imaging Key Laboratory, Systems Biology Theme, Department of Biomedical Engineering, College of Life Science and Technology, Huazhong University of Science and Technology, Wuhan 430074, China

ARTICLE INFO

Article history:
Received 19 October 2017
Received in revised form
21 December 2017
Accepted 25 January 2018
Available online 15 February 2018

Keywords:
Microfluidic chip
Chemical perfusion
Ca^{2+} waves
Dynamic signaling

ABSTRACT

Cell signaling has been recognized as a highly dynamic process. How to capture such dynamics with changes of chemical microenvironment at single cell resolution among cells population without interfering with adjacent cells has been still an immense challenge. Here, we proposed a precision guided microfluidic chemical perfusion strategy for investigating chemical-activated cell signaling via dynamic imaging with high temporal (~12 ms), spatial resolutions and precision. Theory for the microfluidic operation was first established and validated by both numerical simulations and experiments. A computer-aided multi-channel pressure control system was constructed to automatically implement chemical perturbations with various microperfusion times, relaxation times and number of cycles. The width and the position of the chemical microflow could also be precisely controlled with high reliability and accuracy. Investigations of intracellular and intercellular calcium signaling were successfully demonstrated using the proposed method. These results revealed that the precision guided microfluidic chemical perfusion strategy provided a versatile means for cell signaling analysis, which is potentially meaningful in chemical biology, cell biology and pharmacology.

Cell signaling has been recognized as a highly dynamic biological process [1–4]. It involves complicated intracellular regulations from gene regulatory network, and the fluctuations to extracellular microenvironment. To probe these sophisticated dynamics, particularly for single cell-initiated signal propagation among cells population, two critical technologies including high resolution imaging and high precise perturbation are required. Recently, there have been tremendous progresses in high or super resolution imaging [5–8]. However, high precise perturbation for localizing the environmental factor to single cell among cells population without interfering with adjacent cells has been still an immense challenge.

Traditionally, glass micropipettes, U-shaped tube [9], optical uncaging of caged effectors [10], have been applied to alter the cellular environment and to deliver active compounds to biological interfaces. These are simple and useful methods, however, they lack temporal and concentration preciseness, due to the diffusion of the active substrate outside the field of analysis using glass micropipettes and U-shaped tube and limit available photolysis compounds in optical uncaging of caged effectors.

The emerging microfluidic technology offers an opportunity to overcome some of these limitations [11–17]. Particularly, microfluidic systems are capable of handling small amounts of fluids in microchannels, which enables precise and dynamic control over a defined microenvironment, allowing cell signaling events to be manipulated and dynamically characterized. For example, laminar co-flow [18–22], hydrodynamic focusing [23] and pore aided well-defined dosing streams [24,25] are approaches to selective supply chemicals to treat different regions of cells with high spatial resolution [26]. Another strategies including hydrodynamic gating [27,28], pulsing [29], interface shifting [21,30–33], single cell moving between parallel fluid streams [34,35], on/off-chip valves [36] have been applied to control the dynamic microenvironment around cells with high temporal resolution. Compared with the high resolution and precision of the localized mechanical and electrical stimulation, which was positioned either with a microprobe or a microelectrode [37], it was difficult to realize localized biochemical stimulation with high precision (without interfering with adjacent cells) due to the small sizes of attached cell (typically 5–100 μm) and fast diffusion of biochemical reagents (typical

* Corresponding author.
E-mail address: bfliu@mail.hust.edu.cn (B.-F. Liu).
[1] These authors contributed equally to this work.

https://doi.org/10.1016/j.snb.2018.01.195
0925-4005/

diffusion coefficient 1×10^{-9} cm^2/s) [9,15,18,38,39]. Recently, integration microfluidic elements onto an AFM setup [40], termed FluidFM, enabling force-controlled dispersion of a solution containing selected molecules into individual cells within a physiological environment. Furthermore, microfluidic probe (MFP) [41], first reported by the IBM group, combines hydrodynamic focusing with the concept of scanning probes for processing surfaces, which can be used to create chemical gradients on surfaces, protein microarrays, localized staining of cells. These methods accomplish the goal of localizing small molecules to subcellular regions with high precision, however, they required precise handling of micromanipulators, and the fluid flow may be susceptible to disturbances and variations. Based on above mentioned methods, until now, it remains a great challenge to develop such a system with both high spatial-temporal precision and high accuracy control over chemical stimuli to single cell without interfering with adjacent cells.

More importantly, G-protein coupled receptors, such as P2Y receptors, mediated signaling networks regulated a variety of critical physiological processes [42]. Static information on the map of interacting signaling molecules at the basis of such signaling networks exists, unfortunately, little is known about the dynamic operation of these networks because of lacking an efficient method to realize high precise chemical perfusion upon cells.

Using tracer buffer to verify the position of stimulus before and after the experiment could improve the precision [43]. However, frequently changing solution between tracer buffer and stimulation solution manually, led to the complexity and the uncertainty. Alternatively, using the labelled stimulus could overcome this limitation, but it sometimes resulted in cell stimulation at the beginning of the experiment. Inspired by the operating principle of precision-guided missile in military field (Fig. 1a), in this paper, we reported a precision guided microfluidic chemical perfusion strategy for cell dynamic signaling with high spatial (~12 ms) and temporal resolution (infinitesimal pinched width in theory and lateral shifting resolution of 16.3 ± 2.4 μm/0.1 kPa). Theory model was established and validated by both numerical simulations and experiments. A custom-built multi-channel pressure control system was constructed to automatically implement chemical perturbations with various stimulation times, relaxation times and number of cycles. The width and the position of the chemical microflow could also be precisely controlled with high reliability and accuracy. Investigations of intracellular and intercellular calcium signaling were successfully demonstrated using the proposed method. These results revealed that the precision guided microfluidic chemical perfusion strategy provided a versatile means for probing cell signaling, which is potentially useful in chemical biology, cell biology and pharmacology.

1. Experimental

1.1. Materials and reagents

HCl, KCl, NaCl, NaOH, $CaCl_2$, $MgCl_2$, D-glucose and fluorescein were purchased from Sinopharm Chemical Reagent (Shanghai, China). Adenosine 5′-triphosphate disodium salt ($ATPNa_2$), octanol, fibronectin, HEPES, penicillin, streptomycin and dimethyl sulfoxide (DMSO) were purchased from Sigma-Aldrich (St. Louis, MO). Tyrode's solution was prepared with 137 mM NaCl, 5.4 mM KCl, 1.3 mM $CaCl_2$, 1 mM $MgCl_2$, 10 mM Glucose, and 10 mM HEPES HEPES (pH adjusted to 7.2 using NaOH) as the buffer solution. Fluorescein was prepared in the buffer solution at a final concentration of 1×10^{-5} or 1×10^{-7} molL^{-1}. $ATPNa_2$ was prepared in buffer solutions with final concentrations of 10 or 20 μmol L^{-1} as the agonist. Fluo-3/AM (Biotium, USA) in DMSO was diluted in buffer solutions to a final concentration of 10 μmol L^{-1} prior to use. All reagents were of analytical grade or otherwise noted. All solutions were prepared with water purified by the Direct-Q system (Millipore, Bedford, MA, USA) and filtered with 0.22 μm sterilized syringe filters prior to use.

1.2. Cell culture and maintenance

HeLa and NIH-3T3 cells were purchased from the American Type Culture Collection (ATCC, Manassas, VA). Cells were cultured in a 25-cm^2 tissue culture dishes 1–4 days prior to experiments with Dulbecco's modified eagle medium (DMEM, Gibco) supplemented with 10% (v/v) fetal bovine serum (NCS, Gibco), 100 μg mL^{-1} penicillin and streptomycin at 37 °C in a humidified atmosphere of 5% CO_2 incubator (Innova-Co 170; New Brunswick Scientific, Edison, NJ). Cells were harvested by the treatment of 0.25% (w/v) Trypsin-EDTA solution (Gibco) for 1–2 min, and then resuspended in culture media at a final concentration of ~1×10^6 cells/mL prior to use.

1.3. Chip design and fabrication

We designed and fabricated a polydimethylsiloxane (PDMS)-glass hybrid microchip (Fig. S1), in which SI, TI, B1, B2, SO, BO and BO1 corresponded to sample inlet, tracer inlet, buffer inlet 1, buffer inlet 2, sample outlet, buffer outlet and buffer outlet1, respectively. The diagram in Fig. S1a illustrated the overall microchip design with all channels height of 40 μm with dimensions shown in Fig. S1b. Standard soft lithography and rapid prototyping methods were used to fabricate the microchip with polydimethylsiloxane (PDMS) as the structural material [44]. The PDMS layer was then irreversibly bonded to a glass substrate by plasma treatment. Short glass tubes were attached to the entrances of each channel to form the final device (Fig. S1c).

1.4. Apparatus

A schematic of the system setup was shown in Fig. S1, which contained a microfluidic chip, a custom-built multi-channel pressure control module, and a LabView™-based signal control module. The custom-built multi-channel pressure control module was composed of four independent E/P transducers (T-1001, Bellofram, USA), which was used to reduce a supply pressures (compressed nitrogen cylinder) to a regulated output pressure directly proportional to a three-wire voltage input with 0.1% accuracy. A LabVIEW™ (National Instruments, USA) program was written to regulate pressure control module via a PCI controller card (NI6703, National Instruments, USA), and to realize automatic chemical stimulation with varying stimulation times, relaxation times, number of cycles and the width or the position of the agonist.

Experiments were carried out on an inverted fluorescence microscope (IX71, Olympus, Japan) with a CCD camera (Evolve 512, photometrics, USA) for image acquisition (Fig. S1d). The excitation beam was come from a 100 W mercury lamp (USH1030L, Olympus). A filter cube of U-MWIB2 (460–490 nm band-pass filter, 505 nm diachronic mirror, 510 nm high-pass filter, Olympus, Japan) was used to image fluorescein- and Fluo-3-labelled HeLa and NIH-3T3 cells. Fluorescent signals were collected under a 60 × objective (NA 0.7) or a 40 × objective (NA 0.6), finally recorded by a CCD camera or by a photon counter (PMS 400A, B&H GmbH, Berlin, Germany) with 500 Hz sampling rate just for evaluating the temporal resolution of this system. Temperature was maintained at 37 °C using a hot plate (Olympus, Japan) during experiments. Finally, acquired images were further analyzed using image pro plus 6.0, and origin 7.5.

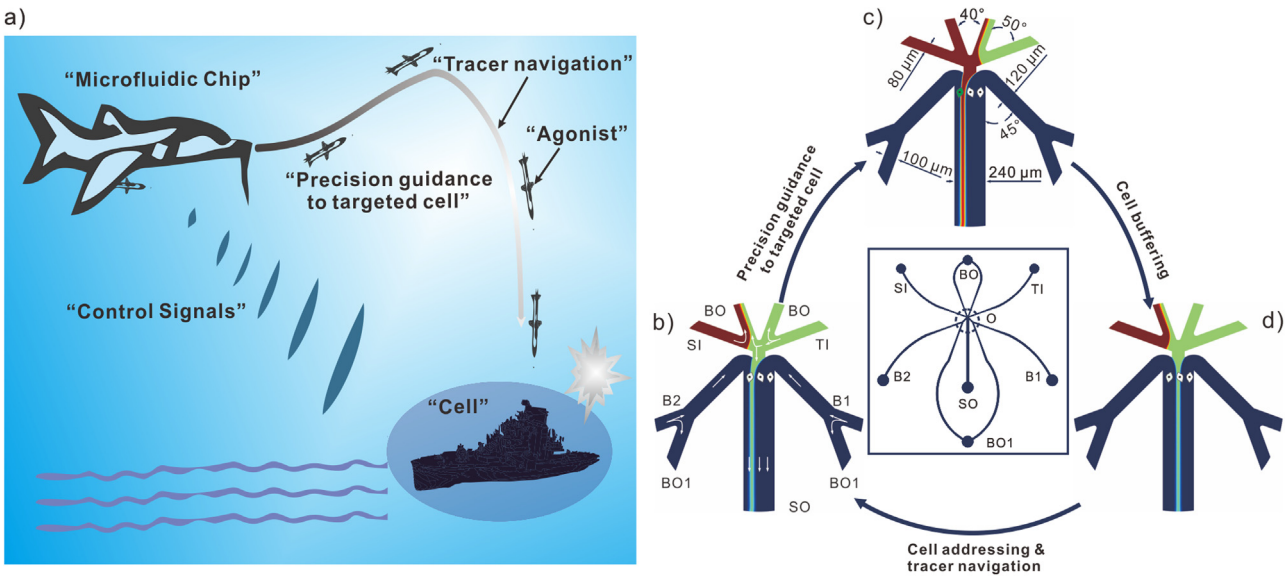

Fig. 1. Precision guided microfluidic chemical perfusion strategy. a) The operating principle of precision-guided missile, b) A green fluorescent dye was used to trace the target cell close to the left border of channel SO. c) An instant switch from the green fluorescent dye to agonist (in red) implements chemical perturbation on the target cell. d) Agonist is switched back to the green fluorescent dye to trace the next cell. (For interpretation of the references to colour in this figure legend, the reader is referred to the web version of this article.)

1.5. Cell seeding and culture in the microfluidic device

Before loading cells, the surface inside the microchannel was chemically modified to enhance cell attachment. The microchip was first treated with oxygen plasma to enhance hydrophilicity. After sterilization with 75% ethanol and incubation at room temperature for 30 min, the microchip was washed gently with Tyrode's solution three times and then incubated with 20 μg mL^{-1} fibronectin (BD Biosciences, Bedford, MA) at 37 °C for 2 h. The microchannel was then sequentially rinsed with buffer solutions and cell culture media.

Cells were seeded in the microchannel using hydrostatic pressures. In brief, culture media of 150 μL were added to reservoir SI, TI and BO. Equal volumes of cell suspensions with a concentration of approximately 1×10^6 cells/mL were added to reservoir SO. Reservoir B1, B2 and BO1 were added with 140 μL culture media. Due to the difference in the height of the fluid in the reservoirs, cell suspensions would flow from reservoir SO to B1, B2 and BO1 and cells would slowly precipitate and finally adhere to the bottom of the microfluidic channel. Following cell seeding, the microchip was gently transferred to a CO_2 incubator for cell culture.

1.6. Calcium imaging

Cells adhered to the bottom of the microchannel were washed gently with buffer solution three times and then loaded with 10 μM Fluo-3/AM solution at 37 °C for 45 min via hydrostatic pressures-driven perfusion. Then the Fluo-3/AM solution was replaced with the buffer solution. The microchannels and reservoirs were filled with 150 μL buffer solution again at 37 °C for another 10 min. Once agonist solution was introduced into the microchannel for stimulating cells locally, fluorescent images were captured by a CCD camera (Evolve 512, Photometrics, USA) at 200 ms interval with an exposure time of 200 ms.

2. Results and discussion

Previously, our group has proposed a gated pinched-flow strategy, by using tracer buffer to verify the position of stimulus before and after the experiments [43]. However, frequently changing solution between tracer buffer and stimulation solution manually, might lead to the complexity and the uncertainty. The cells locating at non-stimulated region could not be activated during the transition state (state switched between OFF and ON) heavily depending on low concentration of ATP and rapid transition time. To overcome such limitations, in this paper, a precision guided microfluidic chemical perfusion strategy was proposed. With the help of innovative structural design, the position of stimulus could be verifed on line using the tracer buffer, which not only simplified the experimental operation, but also improved the precision and accuracy. Upon instant exchange of pressures, only the target cell could be stimulated precisely without perturbing the adjacent cells by precision guidance of tracer buffer, eliminating the potential risk during the transition state in the gated pinched-flow strategy.

2.1. Theoretical model

The schematic representations shown in Fig. 1b–d demonstrate the proposed strategy. Briefly, cells were seeded at the location within 300 μm downstream the intersection O and incubated at 37 °C in 5% CO_2 atmosphere overnight before experiments. Agonist, green fluorescent tracer solution and buffer solution were supplied to reservoir SI, TI and B1/B2 respectively. By controlling the pressures on these four entrances with other channel ports open to atmosphere, a pinched flow of the green fluorescent dye could be manipulated to trace the target cell (Fig. 1b). Upon instant exchange of pressures on SI and TI, the green fluorescent dye was switched to agonist to stimulate the target cell by precision guidance of tracer solution (Fig. 1c). Since the flow pattern of the agonist was the same as the green fluorescent dye, only the target cell would be stimulated precisely without perturbing the adjacent cells. After the pressures on SI and TI were switched back, the agonist was changed to the green fluorescent dye for buffering cells, which could be further manipulated to trace or address the next cell by adjusting the pressures on B1 and B2 (Fig. 1d).

To validate the feasibility of the proposed method, we theoretically investigated the underlying physics. Since the fluid remained laminar in the microchannel (Reynolds number ≈ 1), the pressure

drops in each arm of the microchannel could be described by simplified Hagen-Poiseuille's Law [45]:

$$\Delta P = QR_H \tag{1}$$

where ΔP is the pressure drop between the two ends of the microchannel, Q is the volumetric flow rate and R_H is the hydraulic resistance.

According to the Kirchhoff's current law, the conservation of mass in fluidic circuits implies that the sum of the flows entering into a node should be equal to the sum of the flows leaving out the node. Thus, at knot O,

$$Q_{TI} + Q_{SI} + Q_{B1} + Q_{B2} + Q_{BO} + Q_{BO1} + Q_{SO} = 0 \tag{2}$$

where Q_{TI}, Q_{SI}, Q_{B1}, Q_{B2}, Q_{BO}, Q_{BO1} and Q_{SO} is the volumetric flow rates in the microchannel O-TI, O-SI, O-B1, O-B2, O-BO, O-BO1 and O-SO, respectively.

By substituting Eq. (1) for Q, Eq. (2) can be described as below:

$$\frac{P_{TI}-P_O}{R_{O-TI}} + \frac{P_{SI}-P_O}{R_{O-SI}} + \frac{P_{B1}-P_O}{R_{O-B1}} + \frac{P_{B2}-P_O}{R_{O-B2}} + \frac{P_{BO}-P_O}{R_{O-BO}} + \frac{P_{BO1}-P_O}{R_{O-BO1}} + \frac{P_{SO}-P_O}{R_{O-SO}} = 0 \tag{3}$$

where P_{TI}, P_{SI}, P_{B1}, P_{B2}, P_{BO}, P_{BO1}, P_{SO} and P_O represent the pressures on TI, SI, B1, B2, BO, BO1, SO and O. The hydraulic resistance for the rectangular microchannel can be calculated by Eq. (4) when the aspect ratio (h/w) ≈ 1,

$$R_H = \frac{12\eta L}{wh^3(1-0.63h/w)} \tag{4}$$

where L is the length of the microchannel, η is the dynamic viscosity of the fluid, w and h are width and height of the microchannel, respectively. To simplify the calculation, we assumed that $L_{O\text{-}TI} = L_{O\text{-}SI} = L_{O\text{-}B1} = L_{O\text{-}B2} = L_{O\text{-}BO} = L_{O\text{-}BO1} = L_{O\text{-}SO}$. Some other specific dimensions as shown in Fig. S1a. Thus, the ratio of the hydraulic resistance in the microchannel can be calculated as follows:

$$\begin{aligned} &R_{O-TI} = R_{O-SI} = 2R_{O-BO}, \quad && R_{O-B1} = R_{O-B2} = 2R_{O-BO1}, \\ &R_{O-SI} = 1.36R_{O-B1}, && R_{O-SO} = 0.35R_{O-B1} \end{aligned} \tag{5}$$

Deriving from the Eqs. (3) and (5) with $P_{BO} = P_{BO1} = P_{SO} = 0$ kPa, the pressure at knot O can be obtained:

$$P_O = \frac{0.74(P_{TI}+P_{SI}) + 0.5(P_{B1}+P_{B2})}{8.8} \tag{6}$$

As shown in Eq. (6), if the total pressure at TI and SI is fixed at a constant value and the total pressure at B1 and B2 is fixed at a constant value, P_O would also maintain at constant values. The position of the pinched flow (W_D) was defined as the distance from the left channel wall to the peak center of the fluorescence signal, and the width (W_S) was defined as the distance between the rising and the falling point corresponding to 10% of the highest fluorescence intensity. Since the ratio of the volumetric flow rates is directly proportional to the ratio of the width of the laminar flow in the microchannel, the width (W_S) and the position (W_D) of the pinched-flow can be described as follows:

$$W_S = w\frac{Q_{TI}+Q_{SI}-Q_{BO}}{Q_{SO}} = 0.25w\left(\frac{P_{TI}+P_{SI}-4P_O}{P_O}\right) \tag{7}$$

$$W_D = 0.175w\left(\frac{P_{B1}+P_{B2}-0.7(P_{TI}+P_{SI})-4P_O}{P_O}\right) \tag{8}$$

As shown in Eq. (6)–(8), W_S and W_D can be adjusted by changing the pressures at TI, SI, B1 and B2. Crucially, when the total pressure at B1 and SI is fixed at a constant value and the total pressure at B2 and SO is fixed at a constant value, the P_O, even the W_S and W_D would also maintained at constant values. In this case, instant exchange of pressures on SI and TI won't change the value of W_S and the W_D, indicated that the proposed precision guided microfluidic chemical perfusion strategy was established in principle. Furtherly, numerical simulations shown in Video S1 was also validate the feasibility of the proposed method.

2.2. Temporal resolution of the precision guided microfluidic chemical perfusion strategy

Because the time period could be precisely controlled between the pressure switches, the target cell could be pulsed with a user-defined time span (Video S2). Experiments were first carried out on an inverted fluorescence microscope to investigate the temporal resolution of the proposed chemical perfusion strategy (Fig. S1). Fluorescein with a concentration of 1×10^{-7} M was supplied to reservoir TI and buffer solutions were supplied to reservoir SI, B1 and B2. The pressures on B1 and B2 were both set to 0.5 kPa. The pressures on TI and SI were set to 0.5 and 1.5 kPa, at a constant ratio of 1:3 (Fig. S2). By alternating the pressures on TI and SI, repeated pulsing of fluorescein (injection time, 100 ms; relaxation time, 600 ms) were first carried out to study the repeatability of this method. A relative standard deviation (RSD) of 0.5% (n = 10) was observed for the peak height, indicating an outstanding repeatability for pulse generation (Fig. 2a). By controlling the injection time, pulses of fluorescein with increasing durations could also be achieved (Fig. 2b). A typical 100 ms pulse was shown in Fig. 2c. The rise time and fall time corresponding to 90% change in fluorescence intensity was 24.5 ± 0.4 ms and 27.5 ± 0.3 ms respectively (n = 10), indicating a fast solution exchange. In theory, the solution exchange time is related to the flow rate of fluoresce in the microchannel, hence the total pressures on all the entrances. We next studied the effect of total pressures on both the rise and the fall time. As shown in Fig. 2d, an exponential decrease was observed for both the rise and fall time with increasing pressures, resulting in a minimum solution exchange time of ~12 ms. Considering the adverse impact of shear stress on live cells, we used a total pressure of less than 5 kPa for the following experiments. Under this pressure range, the maximum shear stress on live cells was estimated to be 3.1 Pa, which was less than 3.7 Pa and harmless to HeLa and NIH-3T3 cells [19]. The control experiments also indicated that the shear stress did not induce any significant changes in cell morphology and variations in intracellular Ca^{2+} concentration when the cell was instantaneously stimulated with buffer solutions at a duration of 2 s (Fig. S3). It was worth noting that the maximum shear stress (3.1 Pa) applied in this paper was larger than those in blood vessels (e.g. 1–2 Pa in aorta and 0.1–0.6 Pa in vein). Since the shear stress on cells is related to the changing of pressure drop between the two ends of the microchannel, it could be flexible adjusted by decreasing the input pressures to meet such situations, slightly led to prolonged the solution exchange time.

Subsequently, we attempted use of this chemical pulse generator to monitor calcium signaling via P2Y receptors in HeLa cells. With 5 s pulses of 20 μM ATP and 60 s intervals, a quick decline in the height of the calcium spikes was observed (Fig. S4), indicating desensitization of the P2Y receptors, which consistented with previous reports. In contrast, relatively stable calcium spikes were revealed with 300 ms ATP pulses (Fig. 2e), suggesting minimal receptor desensitization [28]. A possible reason could be that protein kinase C-induced inactivation of the P2Y receptors was largely prevented due to the millisecond ATP pulses. Further consecutive pulses of cells with increasing durations from 500 ms to 60 s showed that calcium spikes evolved from single peak to multiple peaks, a phenomenon known as calcium oscillations. The number of calcium spike could be well defined based on the proposed strategy, which furtherly would likely be an intracellular signal encoding mode to mediate different signal pathway. These results indicated

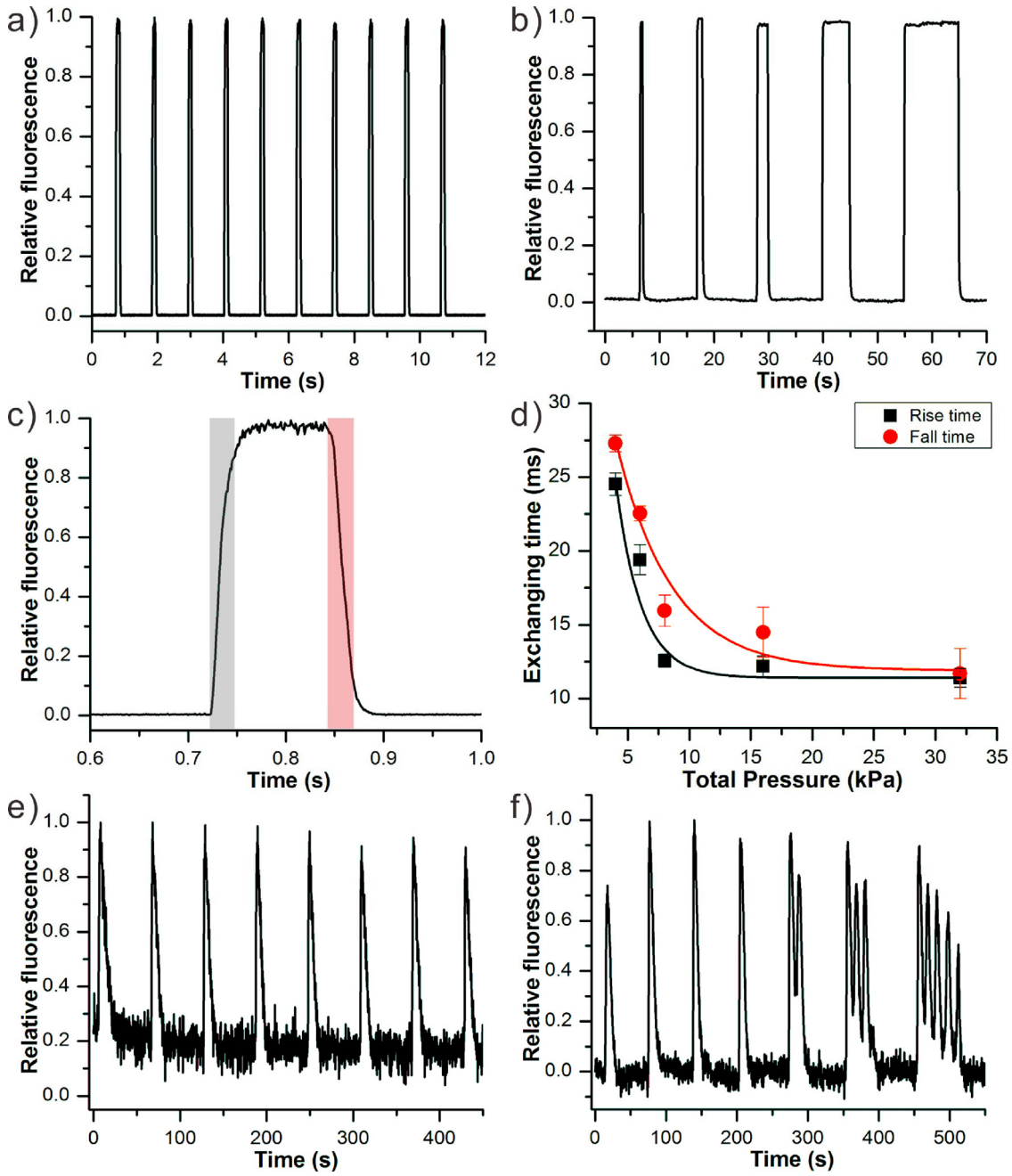

Fig. 2. Temporal resolution of the precision guided microfluidic chemical perfusion strategy. a) Repeated injections of fluorescein with an injection time of 100 ms and a relaxation time of 600 ms. b) Repeated injections of fluorescein with increasing injection times (500 ms, 1 s, 2 s, 5 s and 10 s) and a constant relaxation time of 10 s. c) A 100 ms pulse with rise time and fall time indicated as grey and red area respectively. d) Pressure effect on rise time (black) and fall time (red) fitted with single exponential functions. The pressure ratio on TI and SI were 3:1 during injection and 1:3 during relaxation. Error bars indicate the standard deviation of 5 experiments. e) A single cell response to repeated injections of 20 μM ATP with an injection time of 300 ms and a relaxation time of 60 s. f) A single cell response to repeated injection of 20 μM ATP with increasing injection times (500 ms, 2 s, 5 s, 10 s, 20 s, 40 s, 60 s) and a constant relaxation time of 60 s. (For interpretation of the references to colour in this figure legend, the reader is referred to the web version of this article.)

a high temporal resolution of the proposed strategy, which was suitable for analysis of single cells upon chemical perturbations.

2.3. Spatial resolution of the precision guided microfluidic chemical perfusion strategy

We next investigated the spatial resolution of the proposed method (Video S3). With the pressures on TI and SI fixed at 0.5 and 1.5 kPa (Fig. 3a), the width and the position of the pinched flow could be precisely controlled by adjusting the pressures on B1 and B2. Fluorescein solution with a concentration of 1×10^{-7} M was used to visualize the flow patterns during the experiments. Fig. 3b showed a typical concentration profile across the channel 300 μm downstream the intersection O. Quantitative analyses of the width in relation to the total pressures on B1 and B2 were summarized in Fig. 3c. As a result, the width of the pinched flow decreased linearly with increasing total pressures on B1 and B2. Furtherly, the specific W_S would be chose depend on an actual experiment despite the W_S could be controlled to an infinitesimal width in theory. With the total pressure on B1 and B2 fixed at 2.2 kPa, the position of the pinched flow was found to vary in linear relation to the pressures

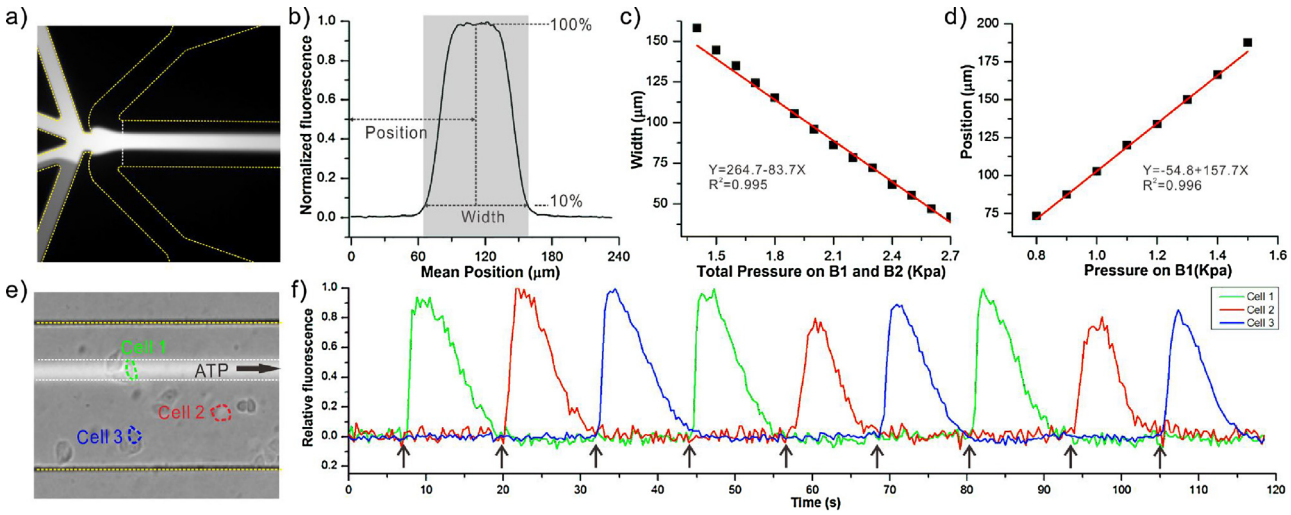

Fig. 3. Spatial resolution of the precision guided microfluidic chemical perfusion strategy. a) A fluorescent image of fluorescein injection. The dotted yellow lines indicate the microchannel geometry. b) Determination of the position and the effective width of the injected agonist. c) The effective width of the injected agonist in linear relationship to the total pressures on B1 and B2. The red line indicates the linear fit to the data. d) The position of the injected agonist in linear relationship to the pressures on B1. The red line indicates the linear fit to the data. e) An image overlay of the attached cells and the fluorescent tracer. Cell 1–3 is indicated with dotted green, red and blue circles respectively. The dotted yellow lines indicate the borders of the microchannel. The dotted white lines indicate the borders of the effective ATP stimulation region. f) A typical recording of intracellular calcium changes in cell 1, 2 and 3 in response to periodical chemical pulses. Black arrows indicate the time point for cell pulsing. (For interpretation of the references to colour in this figure legend, the reader is referred to the web version of this article.)

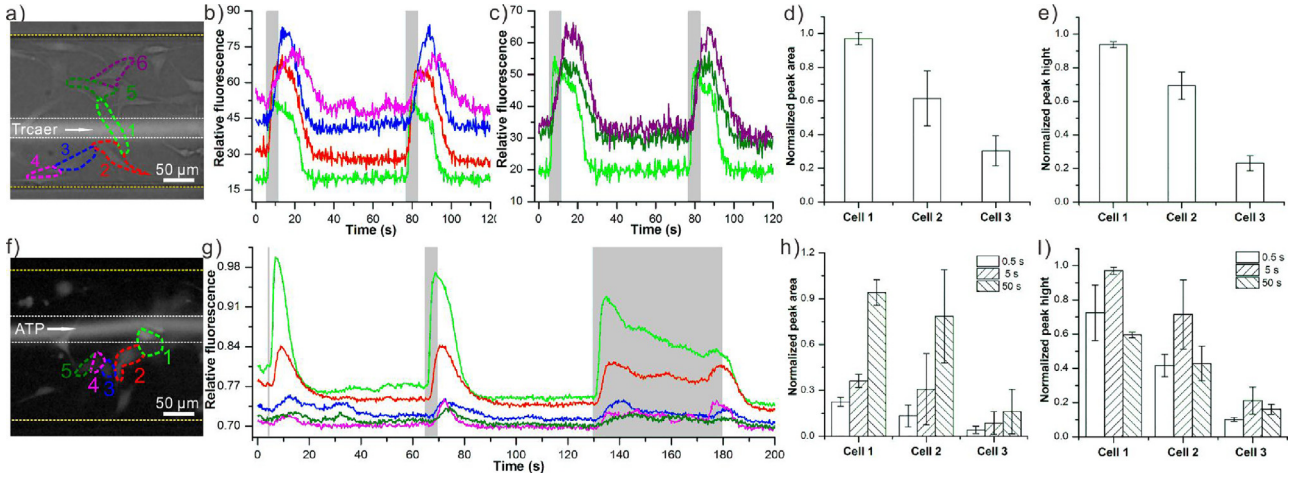

Fig. 4. Precision guided microfluidic chemical perfusion strategy for investigating intercellular signaling. a) A bright image of a cell population. Cell 1–6 is indicated with dotted green, red, blue, magenta, olive and purple circles respectively. The dotted yellow lines indicate the borders of the microchannel. The dotted white lines indicate the borders of the effective tracer navigation or ATP stimulation region. b) A typical recording of intracellular calcium changes in cell 1, 2, 3 and 4 in response to three consecutive ATP pulses on cell 1. The grey shadings indicate the periods of ATP pulses. c) A typical recording of intracellular calcium changes in cell 1, 5, and 6 in response to three consecutive ATP pulses on cell 1. d) The normalized peak area of calcium response in the first three cells during the propagation. e) The normalized peak height of calcium response in the first three cells during the propagation. f) A fluorescent image of a cell population and the fluorescent tracer. Cell 1–5 is indicated with dotted green, red, blue, magenta and olive circles respectively. The dotted yellow lines indicate the borders of the microchannel. The dotted white lines indicate the borders of the effective ATP stimulation region. g) A typical recording of intracellular calcium changes in cell 1, 2, 3, 4 and 5 in response to three consecutive ATP pulses on cell 1. The grey shadings indicate the periods of ATP pulses. h) The normalized peak area of calcium response in cell 1–3 with different ATP pulsing spans. i) The normalized peak height of calcium response in cell 1–3 with different ATP pulsing spans. (For interpretation of the references to colour in this figure legend, the reader is referred to the web version of this article.)

on B1 (Fig. 3d). Typically, a lateral shifting distance of 16.3 ± 2.4 μm was achieved with a pressure change of 0.1 kPa (n = 8).

Above data suggested that both the width and the position of the pinched flow could be precisely controlled. After the target cell is traced down by adjusting the pressures on B1 and B2, an instant switch of the pressures on TI and SI will enable the exchange of tracer solution to agonist, resulting in chemical perturbation of the target cell. We further attempted consecutive pulsing of multiple target cells among a cell population, taking advantages of the high spatial resolution of the proposed methods. As shown in Fig. 3e, three cells were selected for the experiments. The intracellular calcium changes were monitored in real time and the results were shown in Fig. 3f. A supplementary video was provided to illustrate the consecutive pulsing process (Video S4). These results strongly suggested the high reliability and accuracy of the tracer guided cell pulsing strategy.

2.4. The mechanism of agonist-induced intercellular calcium signaling

Intercellular calcium signaling is essential for maintaining cellular functions in multi-cellular organisms. Gap junction is one type of

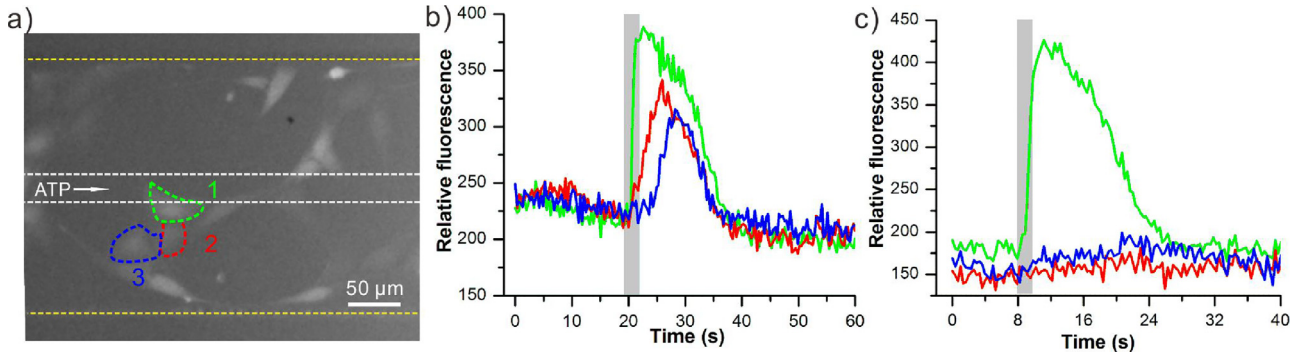

Fig. 5. Inhibition of the propagation of calcium waves by octanol. (a) Contacting cells adhered to the glass in the microchannel. (b) Time course of fluorescence intensity in the three fluo-3-loaded contacting cells (cells 1–3) under localized ATP stimulation to cell 1 for 5 s with a speed of 11.1 $\mu m s^{-1}$. (c) Time course of fluorescence intensity after octanol (10 μM) exposure to cells.

cell–cell connections that allows small signaling molecules to pass between the cells. Gap junction-mediated intercellular calcium signaling is critical to important physiological processes including cell proliferation, differentiation and apoptosis [46,47]. Defects in this signaling pathway may result in hereditary human diseases such as deafness, skin diseases and cataracts [48].

Next, we applied the proposed microfluidic strategy to analyze intercellular calcium signaling among NIH-3T3 cells upon activation of P2Y receptors. In NIH-3T3 cells, there are three subtypes of P2Y receptors $P2Y_1$, $P2Y_2$ and $P2Y_4$ [49]. Previous RT-PCR analysis has shown that $P2Y_2$ are more abundantly expressed than $P2Y_1$ and $P2Y_4$ in NIH-3T3 cells. Since $P2Y_2$ has been proven to be the most sensitive one to ATP (EC50, ~1 μM) among the three subtypes, the response of NIH-3T3 cells to ATP may largely depend on $P2Y_2$ receptors [28,49]. After cell seeding in the observation channel and incubation at 37 °C overnight, adjacent contacting cells at ~300 μm downstream the intersection O were selected for intercellular signaling analysis. As shown in Fig. 4a, cell 1 was chosen for two consecutive stimulations of 10 μmol L-1 ATP (injection time, 5 s; relaxation time, 60 s), and the calcium responses in cell 1–6 were recorded over time. As a result, calcium waves propagated from cell 1–2, 3, 4 and cell 1–5, 6 with a propagation speed of ~11.6 $\mu m s^{-1}$ (Fig. 4b) and ~13.2 $\mu m s^{-1}$ (Fig. 4c), respectively. Another example of calcium wave propagation was shown in Fig. S5. Statistical analyses showed that both the peak area (Fig. 4d) and the peak height (Fig. 4e) decreased gradually along the propagation route, which might result from the desensitization of the purinergic receptors. We further attempted consecutive ATP pulses on cell 1 (Fig. 4f) with increasing durations from 500 ms to 50 s (relaxation time, 60 s). As shown in Fig. 4g, three calcium waves were successfully evoked from cell 1–5 with a propagation speed of ~13.6 $\mu m s^{-1}$, and the calcium spikes evolved from a single peak into multiple peaks in all cells. Statistical analyses showed that the peak area of the calcium spikes in all cells increased with prolonged pulsing spans (Fig. 4h). However, the largest peak height was observed with a pulsing duration of 5s (Fig. 4i). In addition, both the peak area and the peak height decreased gradually along the propagation route at a given pulsing duration, similar to the results observed in Fig. 4c and 4d. To validate whether the calcium propagation among NIH-3T3 cells was mediated via gap junction, cells were pulsed with ATP in the presence and absence of octanol, an inhibitor of Cx43 protein (Fig. 5). As a result, calcium spikes could only be observed in the target cell without propagation to adjacent contacting cells in the presence of octanol, indicating that the calcium waves were effectively inhibited by octanol. These observations confirmed that the calcium signaling was originated by a local regenerative event, such as IP_3 mediated calcium release and dependent upon direct cytosolic transfer of molecules via gap junctions, in contrast to diffusive processes from the point of stimulation.

3. Conclusions

In this work, we demonstrated a novel precision guided microfluidic chemical perfusion strategy providing a versatile platform for studying cell signaling in individual cells or among contacting cells. It was capable of addressing individual cells among a cell cluster without interfering with adjacent contacting cells. The high temporal resolution further allowed pulsing cells with varying durations, which could be a potentially useful tool for chemical biology, cell biology and pharmacology.

Acknowledgements

We gratefully acknowledge the financial supports from National Natural Science Foundation of China (21775049, 21475049, 31471257 and 31700746) and National Key R&D Program of China (2016YFF0100801).

Appendix A. Supplementary data

Supplementary data associated with this article can be found, in the online version, at https://doi.org/10.1016/j.snb.2018.01.195.

References

[1] D. Vaudry, P.J.S. Stork, P. Lazarovici, L.E. Eiden, Science 296 (2002) 1648–1649.
[2] B.N. Kholodenko, Nat. Rev. Mol. Cell Biol. 7 (2006) 165–176.
[3] J.T. Hancock, Br. J. Biomed. Sci. 65 (2008) 205–208.
[4] J. Downward, Nature 411 (2001) 759–762.
[5] J. Lippincott-Schwartz, Proc. Natl. Acad. Sci. U. S. A. 112 (2015) 2630–2632.
[6] M.J. Rust, M. Bates, X.W. Zhuang, Nat. Methods 3 (2006) 793–795.
[7] E. Betzig, G.H. Patterson, R. Sougrat, O.W. Lindwasser, S. Olenych, J.S. Bonifacino, M.W. Davidson, J. Lippincott-Schwartz, H.F. Hess, Science 313 (2006) 1642–1645.
[8] E. Betzig, J.K. Trautman, Science 257 (1992) 189–195.
[9] F. Bradke, C.G. Dotti, Science 283 (1999) 1931–1934.
[10] C. Beta, D. Wyatt, W.J. Rappel, E. Bodenschatz, Anal. Chem. 79 (2007) 3940–3944.
[11] A.R. Wheeler, W.R. Throndset, R.J. Whelan, A.M. Leach, R.N. Zare, Y.H. Liao, K. Farrell, I.D. Manger, A. Daridon, Anal. Chem. 75 (2003) 3581–3586.
[12] F. Guo, J.B. French, P. Li, H. Zhao, C.Y. Chan, J.R. Fick, S.J. Benkovic, T.J. Huang, Lab Chip 13 (2013) 3152–3162.
[13] S. Nahavandi, S.Y. Tang, S. Baratchi, R. Soffe, S. Nahavandi, K. Kalantar-Zadeh, A. Mitchell, K. Khoshmanesh, Small 10 (2014) 4810–4826.
[14] A. Benedetto, G. Accetta, Y. Fujita, G. Charras, Lab Chip 14 (2014) 1336–1347.
[15] J. El-Ali, P.K. Sorger, K.F. Jensen, Nature 442 (2006) 403–411.
[16] R. Dhumpa, M.G. Roper, Anal. Chim. Acta 743 (2012) 9–18.
[17] L. Chingozha, M. Zhan, C. Zhu, H. Lu, Anal. Chem. 86 (2014) 10138–10147.
[18] S. Takayama, E. Ostuni, P. LeDuc, K. Naruse, D.E. Ingber, G.M. Whitesides, Chem. Biol. 10 (2003) 123–130.
[19] B. Kuczenski, W.C. Ruder, W.C. Messner, P.R. LeDuc, PLoS One (2009) 4.

[20] Y.Y. Chiang, J. West, Lab Chip 13 (2013) 1031–1034.
[21] K.R. King, S. Wang, A. Jayaraman, M.L. Yarmush, M. Toner, Lab Chip 8 (2008) 107–116.
[22] C. Bathany, D. Beahm, J.D. Felske, F. Sachs, S.Z. Hua, Anal. Chem. 83 (2011) 933–939.
[23] F. Wang, H. Wang, J. Wang, H.Y. Wang, P.L. Rummel, S.V. Garimella, C. Lu, Biotechnol. Bioeng. 100 (2008) 150–158.
[24] T.J. Hoppe, S.G. Moorjani, J.B. Shear, Anal. Chem. 85 (2013) 3746–3751.
[25] R. Nielson, J.B. Shear, Anal. Chem. 78 (2006) 5987–5993.
[26] B. Meier, A. Zielinski, C. Weber, D. Arcizet, S. Youssef, T. Franosch, J.O. Radler, D. Heinrich, Proc. Natl. Acad. Sci. U. S. A. 108 (2011) 11417–11422.
[27] P. Chen, X.J. Feng, J. Sun, Y. Wang, W. Du, B.F. Liu, Lab Chip 10 (2010) 1472–1475.
[28] J. Sun, P. Chen, X.J. Feng, W. Du, B.F. Liu, Biosens. Bioelectron. 26 (2011) 3413–3419.
[29] P. Sabounchi, C. Ionescu-Zanetti, R. Chen, M. Karandikar, J. Seo, L.P. Lee, Appl. Phys. Lett. (2006) 88.
[30] E. Dahan, V. Bize, T. Lehnert, J.D. Horisberger, M.A.M. Gijs, Lab Chip 8 (2008) 1809–1818.
[31] P. Chen, P. Chen, X.J. Feng, W. Du, B.F. Liu, Anal. Bioanal. Chem. 405 (2013) 307–314.
[32] P. Chen, Y.R. Guo, J. Wang, W. Du, X.J. Feng, B.F. Liu, Sens. Actuators B-Chem. 251 (2017) 112–119.
[33] P. Chen, Y. Guo, X. Feng, S. Yan, J. Wang, Y. Li, W. Du, B.F. Liu, Anal. Chem. 89 (2017) 9209–9217.
[34] J. Olofsson, H. Bridle, J. Sinclair, D. Granfeldt, E. Sahlin, O. Orwar, Proc. Natl. Acad. Sci. U. S. A. 102 (2005) 8097–8102.
[35] J. Olofsson, S.J. Xu, G.D.M. Jeffries, A. Jesorka, H. Bridle, I. Isaksson, S.G. Weber, O. Orwar, Anal. Chem. 85 (2013) 10126–10133.
[36] T. Xu, W.Q. Yue, C.W. Li, X.S. Yao, M.S. Yang, Lab Chip 13 (2013) 1060–1069.
[37] M. Junkin, Y. Lu, J.X. Long, P.A. Deymier, J.B. Hoying, P.K. Wong, Biomaterials 34 (2013) 2049–2056.
[38] J.V. Gerasimenko, Y. Maruyama, K. Yano, N.J. Dolman, A.V. Tepikin, O.H. Petersen, O.V. Gerasimenko, J. Cell Biol. 163 (2003) 271–282.
[39] S. Takayama, E. Ostuni, P. LeDuc, K. Naruse, D.E. Ingber, G.M. Whitesides, Nature 411 (2001) 1016.
[40] A. Meister, M. Gabi, P. Behr, P. Studer, J. Voros, P. Niedermann, J. Bitterli, J. Polesel-Maris, M. Liley, H. Heinzelmann, T. Zambelli, Nano Lett. 9 (2009) 2501–2507.
[41] G.V. Kaigala, R.D. Lovchik, E. Delamarche, Angew. Chem. Int. Ed. 51 (2012) 11224–11240.
[42] P.R. O'Neill, L. Giri, W.K.A. Karunarathne, A.K. Patel, K.V. Venkatesh, N. Gautam, Wiley Int. Rev. Syst. Biol. Med. 6 (2014) 115–123.
[43] P. Chen, X.J. Feng, D.J. Chen, C. Liu, W. Du, B.F. Liu, Sens. Actuators B-Chem. 234 (2016) 583–592.
[44] D.C. Duffy, J.C. McDonald, O.J.A. Schueller, G.M. Whitesides, Anal. Chem. 70 (1998) 4974–4984.
[45] K.W. Oh, K. Lee, B. Ahn, E.P. Furlani, Lab Chip 12 (2012) 515–545.
[46] T.W. White, Science 295 (2002) 319–320.
[47] F.H. Paraguassu-Braga, R. Borojevic, L.F. Bouzas, M.A. Barcinski, A. Bonomo, Cell Death Differ. 10 (2003) 1101–1108.
[48] D.A. Gerido, T.W. White, Biochim. Biophys. Acta-Biomembr. 1662 (2004) 159–170.
[49] G. Burnstock, Curr. Top. Med. Chem. 4 (2004) 793–803.

Biographies

Peng Chen received his Ph.D. degree in Huazhong University of Science and Technology (HUST), China. His research interest focuses on microfluidic-based methods for cell analysis.

Xiaojun Feng received his Ph.D. degree in Biology from the University at Albany, State University of New York in 2006. Thereafter, he moved to HUST, China, continuing his postdoctoral research in the College of Life Science & Technology. He is currently an associate professor at HUST. His research interest includes BioMEMS, microfluidics, point-of-care testing and mass spectrometry-based proteomics.

Shuangqian Yan received his Ph.D. degree in Huazhong University of Science and Technology (HUST), China. His research interest focuses on microfluidic-based methods for tumor diagnosis and therapy.

Yiran Guo is pursuing her doctoral degree in HUST, China. Her research interest focuses on the development of microfluidic devices for cell analysis.

Jie Wang is a Ph.D. candidate in HUST. Her main research interest focuses on microfluidic-based methods for POCT and exosomes analysis.

Yiwei Li received his Ph.D. degree in Huazhong University of Science and Technology (HUST), China. His research interest focuses on microfluidic-based methods for biological applications and bioengineering.

Dongjuan Chen received his Ph.D. degree in HUST, China. Her research interest focuses on the development of microfluidic chips for investigating single-cell proteomics.

Wei Du received his Ph.D. degree in Biology from Wuhan University, China. He is currently an associate professor at HUST. His research interest focuses on optical imaging of C. elegans.

Bi-Feng Liu received his Ph.D. degree in Analytical Chemistry from Wuhan University (China) in 1999 and continued his postdoctoral research in the College of Life Science. From 2001, he moved to Japan and worked in Prof. Terabe's group (Japan) as a JSPS postdoctoral fellow. He joined HUST as a professor in 2003. He is now serving as deputy Dean of the College of Life Science & Technology. His research focuses on systems biology-oriented analytical science in the areas of mass spectrometry coupled micro-separation, microfluidics and molecular imaging